

Probing the nature of the K-rotor in unimolecular reactions: Scalar and vector correlations in the photodissociation of NCNO

W. Sean McGivern and Simon W. North

Citation: *The Journal of Chemical Physics* **116**, 7027 (2002); doi: 10.1063/1.1462581

View online: <http://dx.doi.org/10.1063/1.1462581>

View Table of Contents: <http://scitation.aip.org/content/aip/journal/jcp/116/16?ver=pdfcov>

Published by the [AIP Publishing](#)

Articles you may be interested in

[Vibrationally mediated photodissociation of ethene isotopic variants preexcited to the fourth C–H stretch overtone](#)
J. Chem. Phys. **125**, 133301 (2006); 10.1063/1.2217743

[Infrared overtone spectroscopy and unimolecular decay dynamics of peroxyxynitrous acid](#)
J. Chem. Phys. **122**, 094320 (2005); 10.1063/1.1854094

[Resonance-state selective photodissociation of OCS \(\$2\ 1\ \Sigma^+\$ \): Rotational and vibrational distributions of CO fragments](#)
J. Chem. Phys. **113**, 6598 (2000); 10.1063/1.1310606

[State to state recoil anisotropies in the photodissociation of deuterated ammonia](#)
J. Chem. Phys. **109**, 7659 (1998); 10.1063/1.477411

[Vector and scalar correlations in statistical dissociation: The photodissociation of NCCN at 193 nm](#)
J. Chem. Phys. **106**, 60 (1997); 10.1063/1.473023



Probing the nature of the K -rotor in unimolecular reactions: Scalar and vector correlations in the photodissociation of NCNO

W. Sean McGivern and Simon W. North^{a)}

Department of Chemistry, Texas A&M University, 3255 TAMU, College Station, Texas 77842

(Received 13 November 2001; accepted 29 January 2002)

The photodissociation dynamics of thermal NCNO at 520 and 532 nm have been examined using transient frequency modulation Doppler spectroscopy to measure state-selected CN scalar and vector correlations. Previous work has suggested that the global vibrational and rotational distributions may be described using separate statistical ensembles/phase space theory (SSE/PST). We find that the correlated vibrational and rotational distributions are well described by SSE at 520 nm if the K -rotor is considered inactive. At both wavelengths studied, the correlation between the velocity and the rotational angular momentum vector of the CN product is found to be described by phase space theory with no restriction of the projection of the rotational angular momentum vectors along the relative velocity axis. This is indicative of approximate K -scrambling at the transition state, and a discussion of these results in light of the evolution of the K -quantum number is provided. © 2002 American Institute of Physics. [DOI: 10.1063/1.1462581]

I. INTRODUCTION

NCNO has become a benchmark molecule for the study of barrierless reactions, and the visible photodissociation of this molecule has been the subject of numerous experimental^{1–9} and theoretical^{10–12} studies. Absorption of light with wavelengths shorter than 585.3 nm corresponds to a transition from ground electronic state NCNO to the first excited singlet state (S_1). For photolysis wavelengths longer than 450 nm,⁷ the system internally converts back to the S_0 state, where dissociation occurs along a barrierless potential to form products in their electronic ground states.³ Previous experimental work has focused primarily on the measurement of global vibrational and rotational distributions for both the CN and NO fragments at wavelengths corresponding to 0–5000 cm^{-1} above the dissociation threshold. The global rotational distributions were found to be well-described by phase space theory¹³ (PST), but the measured vibrational branching ratios were hotter than predicted by PST.

To explain these observations, Wittig and co-workers have proposed a theory called separate statistical ensembles (SSE), in which vibrational excitation of the products was derived strictly from the vibrational degrees of freedom of the parent and was decoupled from the parent rotational degrees of freedom.¹⁴ Physically, such a system can be realized if the conserved modes randomize energy only until the system reaches the inner transition state and the transitional modes exchange energy until the outer transition state is reached. The SSE/PST predictions were found to reproduce the global vibrational and rotational distributions of CN and NO products over a range of wavelengths.^{5,7} Correlated speed distributions, which provide a much more stringent test of the vibrational partitioning, were measured by Qian

et al. using laser induced fluorescence (LIF) to probe the CN fragments and were well-described by SSE.⁸ However, the large linewidth of the LIF probe laser relative to the width of the fragment Doppler profiles limited their overall resolution.

Recent studies have demonstrated that the correlation between the fragment velocity vector, \mathbf{v} , and the rotational angular momentum vector, \mathbf{J} , can provide insight into the torques on the departing fragments during dissociation. Although these were initially applied to the investigation of direct dissociation processes, even in a purely statistical dissociation that is well-described by PST, one should expect $\mathbf{v}-\mathbf{J}$ correlations as a consequence of energy and angular momentum conservation. Deviation from this trivial case can be used as a probe of dynamical constraints. Of particular interest is whether the $\mathbf{v}-\mathbf{J}$ correlation can provide insight into the role of the K -rotor energy, a subject of considerable importance in unimolecular reaction theory.¹⁵ It is currently unclear whether the K -rotor should be treated as adiabatic, requiring its angular momentum to be conserved throughout the reaction, or whether it should be allowed to couple into the reaction coordinate. In the case of a prolate symmetric top, rotation about the symmetry axis, which can be related to the relative velocity axis in the axial recoil limit, is small even though the overall angular momentum is large. K -conservation restricts the available phase space by removing states in which the fragments have a large projection of the angular momentum on the relative velocity axis (helicoptering motion). Since these states contribute to a positive $\mathbf{v}-\mathbf{J}$ correlation, the overall correlation becomes more strongly negative. In a K -scrambled system, one recovers the less polarized PST $\mathbf{v}-\mathbf{J}$ correlation. Though we consider the correlation between \mathbf{v} and \mathbf{N} , the nuclear rotational angular momentum vector, we neglect the difference between \mathbf{N} and the spin-coupled angular momentum \mathbf{J} , and refer to the correlation as a “ $\mathbf{v}-\mathbf{J}$ correlation” to retain common usage.

In recent years, there has been a steady exodus from the

^{a)}Electronic mail: swnorth@tamu.edu

highly averaged environment of the room temperature bulb towards the rarefied environment of the molecular beam. The molecular beam is ideally suited to photodissociation experiments in many ways, significantly reducing thermal averaging effects, and, in some instances permitting state-to-state studies. However, the use of a jet-cooled ensemble characterized by low rotational temperatures precludes the study of certain facets of photodissociation processes. The study of the nature of the K -rotor requires a broad population of the parent rotational quantum states in order to sample a large region of phase space effectively. In a thermal system, the additional angular momentum restrictions imposed by conservation of the K -rotor energy severely limit the available phase space. The differences in the observed dynamics corresponding to these two cases are marked, providing a robust method for determining the extent of K -scrambling. In a jet-cooled sample, the available phase space is significantly limited by the parent rotational distribution irrespective of the nature of the K -rotor, and differences between the predicted $\mathbf{v}-\mathbf{J}$ correlations in the K -scrambled and K -unscrambled cases are minimal. The parent rotational energy also plays a role in testing the applicability of SSE to specific systems. If the K -rotor is active the initially well-defined vibrational energy distribution will blur as energy is exchanged between the rotational and vibrational reservoirs, resulting in a markedly different product vibrational energy distribution. This difference should be particularly significant in the correlated vibrational branching ratios. The study of room temperature samples also serves a more practical function. A correct description of energy partitioning to systems relevant in atmospheric, interstellar, and combustion chemistry necessarily requires the application of statistical theories to thermal systems. Detailed tests of these theories on thermal samples are thus desirable to enable their widespread application.

In the present work, we have examined the 520 and 532 nm photodissociation of NCNO at 295 K using transient frequency modulation (FM) Doppler spectroscopy. As shown in previous studies, this technique is ideal for studying both scalar and vector correlations in barrierless dissociation processes.¹⁶⁻¹⁸ A single mode diode laser (<1 MHz) is used to probe the Doppler line shapes, providing velocity resolution superior to pulsed ultraviolet techniques. The transient FM technique allows a detailed study of correlated vibrational branching ratios for different CN states, providing a stringent test of the applicability of SSE. In addition, we have measured $\mathbf{v}-\mathbf{J}$ correlations at both 520 and 532 nm for several CN rotational states. Both measurements provide a means to probe the evolution of the K -rotor energy during the dissociation.

II. EXPERIMENT

The transient frequency modulation absorption spectrometer has been described in detail previously,^{18,19} and we present only the salient features of the experiment. CN radicals arising from the photodissociation of NCNO were probed using the output of a tunable diode laser that was frequency modulated at $\omega_m = 192$ MHz by a resonant phase modulator. The CN radicals were detected on Q_1 - and R_1 -branch lines of the $A-X$ electronic transition in the 780-

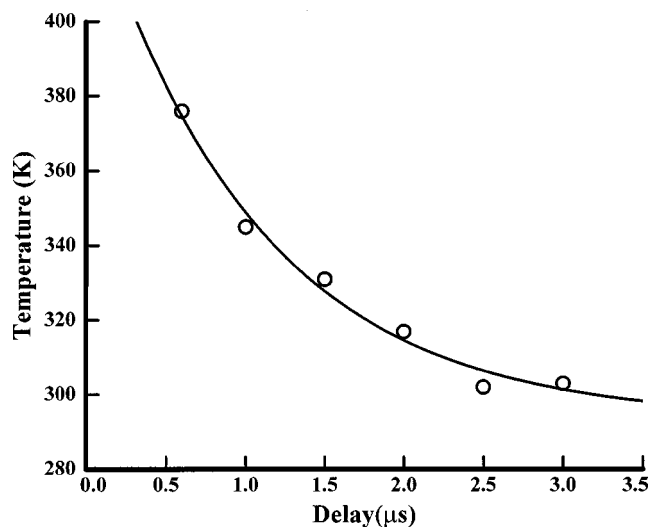


FIG. 1. Fragment internal temperature as a function of delay time for the 532 nm photodissociation of NCNO at 900 mTorr. The circles represent the temperatures of a translational Gaussian that best fit the data for a 150 ns gate as a function of time. The solid line is an exponential fit and is primarily intended to guide the eye. The system appears to come to room temperature (295 K) within several microseconds following the photolysis pulse.

820 nm wavelength range. The 520 and 532 nm photolysis beams were the output of a Nd:YAG-pumped dye laser operating with Coumarin 500 dye. Under the conditions of the present experiment, the modulated near-infrared probe beam may be approximately represented as a combination of three distinct frequencies, separated by ω_m . Preferential absorption of one of these frequencies induces a beat signal on the overall beam intensity, which is detected with a fast photodiode. The beat signal is then amplified and separated using standard phase-sensitive RF electronics into in-phase (I) and quadrature (Q) components with respect to the mixing oscillator. The resulting time-dependent decays are stored as a function of laser wavelength, providing a two-dimensional data set in both time and frequency. In order to ensure that only nascent fragments are contributing to the observed spectra, the Doppler line shapes are generated using signal from only the first 100 ns following photolysis.

In order to quantify the initial parent temperature, time-dependent Doppler spectra were measured for NCNO buffered to ~ 900 mTorr with argon and fit to thermal Gaussian distributions as a function of time. Shown in Fig. 1 are the temperatures of the best-fit Gaussian distributions for Doppler profiles measured at each time using a gate width of 150 ns. The solid line is a best-fit exponential function that is intended to guide the eye. The system returns to room temperature within several microseconds, ensuring that the parent molecules are completely thermalized between laser shots at 10 Hz even at the low sample pressures of the present experiment.

The NCNO sample was synthesized by condensing NOCl on AgCN and collecting the gas above the mixture after approximately 10 min.²⁰ The NOCl reagent was prepared by dripping a concentrated solution of NaNO_2 into concentrated HCl and collecting the evolved gas.²¹ NOCl and NO_2 impurities were removed from the NCNO sample

by trap-to-trap distillation from a dry ice/acetone bath. Samples were prepared at the beginning of each day and were held at $-78\text{ }^\circ\text{C}$ during the experiment. NCNO was introduced neat into the reaction bulb through a needle valve adjusted to provide total pressures of 20–30 mTorr.

III. RESULTS AND ANALYSIS

The absolute phase of the beat signal with respect to the local oscillator used for mixing is unknown, and the resulting I and Q components are linear combinations of the FM absorption and dispersion signals. These I and Q signals were corrected using a recursive method described previously²² to provide pure absorption and dispersion line shapes. FM absorption line shapes were used for the analysis for all rotational states studied.

A. Vector correlations

The determination of $\mathbf{v}-\mathbf{J}$ correlations from the differences between Q - and R -branch absorption lines has been discussed previously¹⁶ and only a brief overview will be given here. Using the bipolar moment theory of Dixon,²³ the Doppler line shape in the absence of any laboratory alignment is given by¹⁶

$$D(w) = \int_{|w|}^{\infty} \frac{1}{2v} [1 - h^{(2)} \beta_0^0(22)_v P_2(w/v)] v^2 f(v) dv,$$

where $P_2(x)$ is the second Legendre polynomial, $\beta_0^0(22)_v$ is the velocity dependent $\mathbf{v}-\mathbf{J}$ correlation given by $\langle P_2(\mathbf{v}\cdot\mathbf{J}) \rangle$, $v^2 f(v)$ is the laboratory speed distribution, $h^{(2)}$ is $+1$ for a Q -branch transition, and $-J/(2J+3)$ for a R -branch line, and w is the projection of the laboratory velocity, v , on the probe laser axis. For \mathbf{v} perpendicular to \mathbf{J} , $\beta_0^0(22)_v = -0.5$, and $\beta_0^0(22)_v = 1.0$ for \mathbf{v} parallel to \mathbf{J} . Previous studies on similar systems using the transient FM technique typically used data that had been inverted to pure absorption space for the determination of the $\mathbf{v}-\mathbf{J}$ correlation.^{16,18,24} Shown in Fig. 2 are overlapped Q - and R -branch FM absorption spectra for $N=11$ and 24. The differences between the Q - and R -branches are extremely small, and errors in the inversion due to slight noise in the FM data lead to errors in the measured $\mathbf{v}-\mathbf{J}$ correlation. We have therefore chosen to fit the Q - and R -branches in FM space. The R - and Q -branch lines were simultaneously fit using a simplex minimization of the overall χ^2 with three parameters,²⁵ two of which are used for a translational energy distribution of the form,

$$\left(\frac{v}{v_{\max}} \right)^a \left(1 - \frac{v}{v_{\max}} \right)^b,$$

with a third parameter representing the $\mathbf{v}-\mathbf{J}$ correlation.

There is no *a priori* reason to expect that a single value of $\beta_0^0(22)$ can describe the angular momentum polarization effectively. We have examined the effects of the velocity dependence on the overall fits by using a linear model for $\beta_0^0(22)_v$. Though this provided an improvement by approximately a factor of 2 in the total χ^2 values, the average values of $\beta_0^0(22)$ from the linear model were within ± 0.005 to the best-fit constant values for all lines studied. Therefore, we have chosen to report only the velocity independent values in

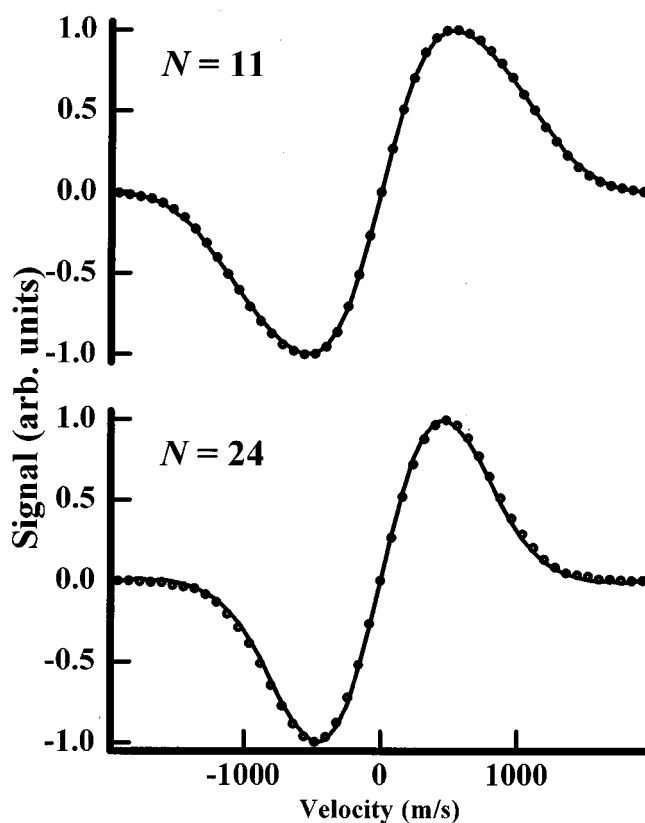


FIG. 2. FM Doppler absorption profiles for $N=11$ and $N=24$ at 532 nm. The circles represent the Q -branch absorption data, and the lines represent R -branch absorption data.

the present work. Similar treatments have been utilized in previous studies and have provided good fits to observed spectra,^{16–18,26} though the neutral time-of-flight apparatus utilized by Wodtke and co-workers had sufficient resolution to differentiate a velocity dependence to the $\mathbf{v}-\mathbf{J}$ parameter of CO from the 308 nm photolysis of ketene.²⁷ To account for slight variations in step size of the laser wavelength, we have examined the difference between the R - and Q -branch lines at late times and adjusted the widths to account for minor differences.²⁸ The solid and dashed lines in Fig. 2 show absorption data for R - and Q -branches, respectively, for $N=11$ and 24. The R - and Q -branch spectra are very similar, especially for $N=11$, which is indicative of a $\mathbf{v}-\mathbf{J}$ correlation near zero. The experimentally determined $\mathbf{v}-\mathbf{J}$ correlations for the measured lines are shown in Fig. 3 as open circles and are found to be small and to vary little with N .

B. Scalar correlations

Previous studies by Pfab *et al.*¹ and Wittig and co-workers^{2,3} have determined global vibrational, rotational, and electronic energy distributions for both CN and NO for room temperature NCNO at several wavelengths throughout the visible absorption region. The distributions were found to be in good agreement with PST results for low values of N at 532 nm and 549 nm. PST was found to underestimate the

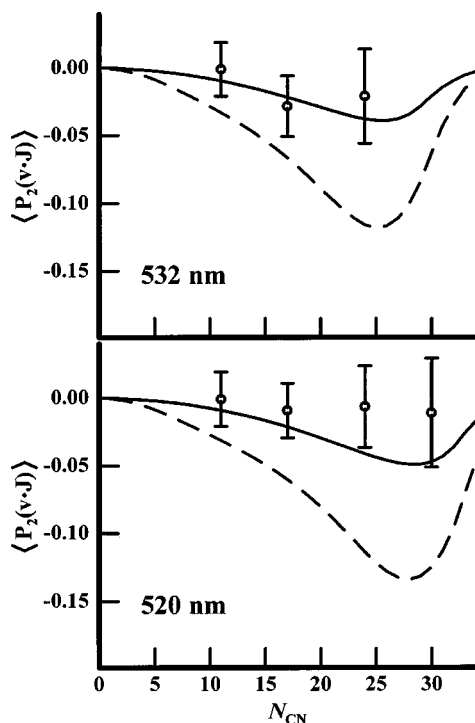


FIG. 3. Measured and calculated values for $\beta_0^0(22)$ for several detected CN rotational states derived from NCNO photodissociation at 532 nm (upper panel) and 520 nm (lower panel). The open circles represent the experimentally determined v - J correlations. The solid and dashed lines are $\beta_0^0(22)$ values calculated using quantum PST for unrestricted Λ and $|\Lambda|$ restricted to values less than or equal to 5, respectively.

population of the higher N states at both wavelengths, likely due to dissociation from vibrationally excited parent molecules.

For each of the CN rotational lines measured in the present work, PST was used to generate the coincident NO fragment rotational distributions. Vibrational averaging was accomplished using a Beyer-Swinehart direct state count algorithm to determine the vibrational energy distribution of the parent molecule at 295 K.²⁹ A Boltzmann average over the parent thermal rotational energy was explicitly included, and the average energy of $|K|$ was included in the available energy. A full Boltzmann average for the K -rotor energy was tested, but no significant deviation was observed from the line shapes simulated by changing only the available energy. In order to simplify the analysis, NCNO was considered to be a prolate symmetric top with rotational constants of 0.175 cm^{-1} and 2.71 cm^{-1} as noted below. For all of the simulations, the population of the $\text{NO}(^2\Pi_{1/2})$ and $\text{NO}(^2\Pi_{3/2})$ spin-orbit states were assumed to be equal. Qian *et al.* have observed systematic deviations from this limit for high N states at approximately 515 nm,⁸ but these deviations were minor for $N < 30.5$. A centrifugal barrier was included in the PST calculations in which the maximum value of the orbital angular momentum, l_{max} , was given by

$$l_{\text{max}}(l_{\text{max}} + 1)\hbar^2 = 6\mu C_6^{1/3}(E_T/2)^{2/3},$$

where C_6 is the attractive potential term from a Lennard-Jones potential,³⁰ μ is the reduced mass of NCNO, and E_T is the relative translational energy of the CN and NO

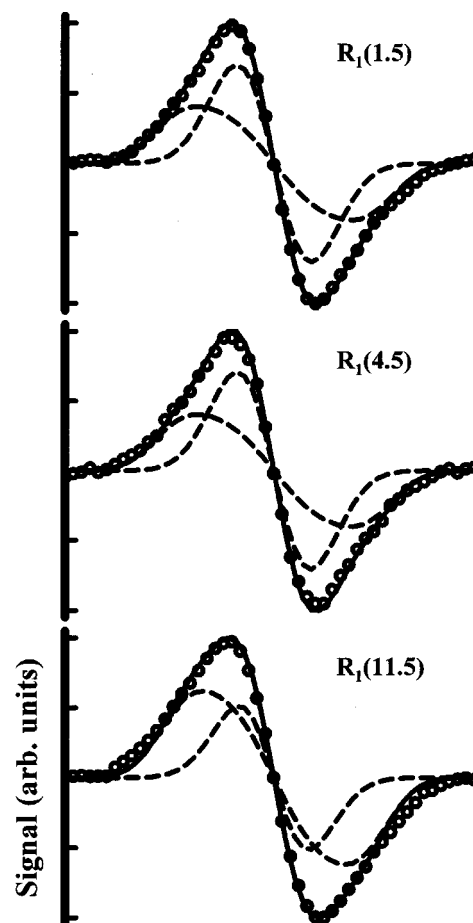


FIG. 4. R -branch Doppler line shapes for $N=1, 4,$ and 11 from the photodissociation of NCNO at 520 nm. The circles represent the experimental data. The solid line is the total fit, and the dashed lines represent contributions from coincident fragments in $v=0$ and $v=1$ vibrational states.

fragments.³¹ From each calculated PST rotational distribution, a velocity distribution was calculated and used to generate the correct Doppler absorption line shape, which was subsequently converted to FM space for comparison with the data.²²

The relative weightings of the Doppler line shapes corresponding to the coincident vibrational components were adjusted to provide the best fits to the measured spectra. Figure 4 shows typical R -branch line shapes for three different CN rotational states derived from NCNO at 520 nm. The solid line is the overall fit to the data that minimizes the χ^2 , using the experimentally determined v - J correlation and the dashed lines are the individual Doppler line shapes that represent the $v=0$ and $v=1$ components. The shapes of the individual lineshapes are significantly different for different values of N , indicative of a strongly changing vibrational branching ratio. As is evident from the figure, the differences between the simulated line shapes for the individual vibrational components are large, providing a robust method for determination of the coincident vibrational branching fractions for each CN rotational state.

Figure 5 shows the vibrational branching fractions determined from the CN lines measured in this study at 520 nm. For the purposes of comparison, correlated vibrational

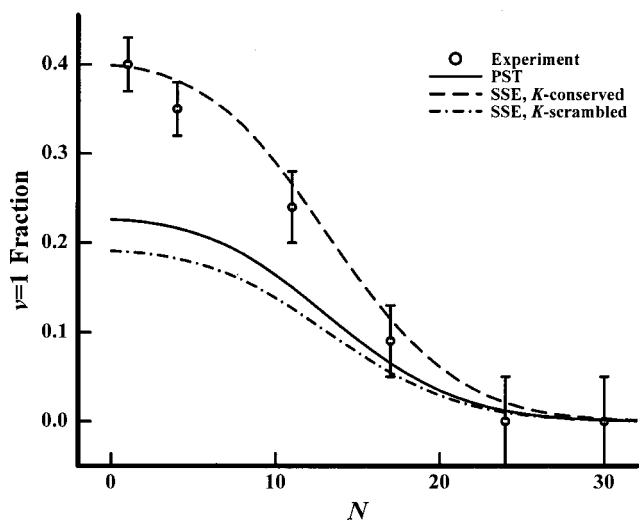


FIG. 5. Correlated vibrational fractions of coincident NO fragments in $v=1$ for the 520 nm photodissociation of NCNO. Circles represent the best-fit values to the experimental data. The solid line represents the PST prediction, the dashed line is the K -conserved SSE prediction, and the dotted-dashed line is the K -scrambled SSE prediction.

branching fractions were calculated using PST as a function of the detected CN rotational state. The “SSE, K -conserved” predictions are the PST predictions scaled by the ratio of the global SSE vibrational branching fraction to the PST global fraction when K is conserved at the inner transition state. The details of the K -rotor treatment within the SSE model are given below. The SSE predictions are in very good agreement with the experimental vibrational branching fractions. For most of the lines examined, both Q - and R -branch line shapes were fit independently, and the branching fractions typically differed by <0.02 between the two lines. The Q -branch lines for $N=4$ and $N=1$ are strongly overlapped with one another and their corresponding satellite transitions,³² and no attempt was made to fit these branches. The $N=30$ line is near the threshold for formation of products from cold NCNO molecules at 520 nm and has contributions from dissociation of highly vibrationally and rotationally excited parent molecules. Although no evidence of a coincident $v=1$ contribution was observed, the high N line shapes were slightly wider than the simulated spectra. These states are extremely sensitive to subtle deviations of the parent vibrational distribution and may contain a larger contribution from vibrationally excited parent molecules than expected from a pure Boltzmann distribution.

IV. DISCUSSION

A. The nature of the K -rotor at the outer transition state

A fundamental tenet of statistical theories of unimolecular dissociation is the ergodic hypothesis, where only a handful of constants of motion are required to fully describe the dissociation rates. Rice–Ramsperger–Kassel–Marcus (RRKM) theory, which provides a powerful means to calculate microcanonical rate constants, generally specifies only the excess energy and the total angular momentum of the

parent molecule and transition state. However, Hase has noted recently that the nature of the K -rotor remains a particularly vexing problem: Can K be considered a good quantum number throughout the dissociation, or does Coriolis coupling result in partial or complete mixing?¹⁵ When K remains a good quantum number, the angular momentum in the K -rotor must be conserved. The additional conserved quantity must therefore be incorporated into statistical theories to correctly describe the reaction rates. A further complication arises from the potential disparate natures of the K -rotors in the reactant and transition state, which may be individually K -conserved or K -scrambled.²⁹

Statistical v - J correlations may be predicted effectively using PST in which the angular momentum states are expanded into a helicity basis.³³ In this basis, the quantum states are indexed by helicity quantum numbers representing the projection of the fragment angular momenta on the relative velocity axis. If the molecule dissociates in the axial recoil limit and the dissociation axis coincides with the long symmetric top axis, the total helicity, Λ , may be associated with the K quantum number.³⁴ Since the individual helicity quantum numbers are bound by the fragment rotational quantum numbers, $|\Lambda|$ is strictly bound by the parent rotational quantum number, J_0 . Although $|K|$ is also bound by J_0 , the nature of the K -distribution imposes an additional constraint. For a prolate symmetric top, the distribution of K quantum numbers is Gaussian and peaked around $K=0$. As such, for moderately large values of J_0 , the total helicity will be constrained by K to values well below J_0 for situations in which K is a good quantum number. We have chosen to treat NCNO as a prolate symmetric top with $A=2.71$ cm^{-1} and $\tilde{B}=(B+C)/2=0.175$ cm^{-1} , providing an average value for $|K|$ of 5 at 295 K.³⁵ The calculation of the v - J correlations when $|\Lambda|$ is both unrestricted and when it is limited to a small value by the parent K distribution provides two distinct simulations that, when compared to measured v - J correlations, can differentiate between K -conserved and K -scrambled models.

We have performed phase space theory calculations in the helicity basis (quantum PST) to determine the values of $\beta_0^0(22)$ for the range of CN rotational states of interest using both Λ -unrestricted and Λ -restricted ($|\Lambda|\leq 5$) models.³³ The thermal averaging used was similar to that used to determine the vibrational branching ratios. Application of quantum PST provides center-of-mass (COM) v - J correlations, which are related directly to the K -distribution at the transition state in the axial recoil limit. However, the thermal translational and rotational motion of the parent molecules degrades these values beyond the transition state, and this degradation must be incorporated into the simulations for comparison to the experimental values. Thermal translational and rotational motion reorients the center-of-mass velocity vector, blurring the center-of-mass v - J correlations. The details of the thermal translational depolarization calculations may be found in Ref. 33. The rotational depolarization mechanism has not been treated previously, and we have developed a simple model to describe its effects, which is shown in the Appendix. The results of the fully degraded laboratory-frame quantum PST calculations are shown as the solid ($|\Lambda|$ -

unrestricted) and dashed ($|\Lambda| \leq 5$) lines in Fig. 3. The thermally degraded $\mathbf{v}-\mathbf{J}$ correlations initially become stronger with increasing values of N , consistent with the behavior of the COM $\mathbf{v}-\mathbf{J}$ correlations. However, the effect of the thermal degrading becomes more significant at lower speeds, causing the values of $\beta_0^0(22)$ to approach zero for the highest detected rotational states. As shown in Fig. 3, the Λ -restricted values of $\beta_0^0(22)$ provide a poor fit to the observed $\mathbf{v}-\mathbf{J}$ correlations at both 520 and 532 nm. However, the fully averaged PST values of $\beta_0^0(22)$ reproduce the observed values well at both wavelengths. The ability of the Λ -unrestricted simulations to reproduce the experimental $\mathbf{v}-\mathbf{J}$ correlations is strongly indicative of approximate K -scrambling at the transition state.

Several factors may contribute to the slight deviations of the observed $\beta_0^0(22)$ from the predicted Λ -unconstrained values. In NCNO, the dissociation axis does not coincide with the symmetric top axis used to calculate the rotational constants, which lies along the NC and NO centers-of-mass. As a result, the correspondence between the total helicity and the K quantum number is not necessarily strict. In addition, the approximate semiclassical treatment of the rotational depolarization factor likely fails to capture some of the more subtle depolarization effects. If the fragment rotational states are “frozen-out” earlier along the reaction coordinate than considered in our calculation, the rotational depolarization would be more severe. The predicted correlations therefore may be expected to slightly overestimate the strength of the measured $\mathbf{v}-\mathbf{J}$ correlations. Additional experiments, already underway, using a pulsed slit-jet should reduce the uncertainty in the measured $\mathbf{v}-\mathbf{J}$ correlations.

B. The nature of the K -rotor at the inner transition state

Both photoexcitation and chemical activation processes can produce rotationally and vibrationally excited product molecules. The partitioning of this excess energy can have a significant effect on the subsequent reactivities of the product molecules, and an understanding of the relevant energy partitioning is therefore necessary for modeling the complex reaction pathways common in atmospheric, combustion, and interstellar chemistry. In a purely statistical dissociation the product state distributions are determined by the degeneracies of the product molecules and the available energy. This behavior is precisely that described by PST, and is usually realized for energies very close to the dissociation threshold, where the number of available states is small. Deviations from this behavior are indicative of dynamical constraints on the dissociating system. The determination of these dynamical constraints is important in determining the overall energy partitioning, which, in turn, leads to a fuller understanding of processes that produce excited radicals.

State-specific photodissociation studies, typically probing global vibrational and rotational distributions of one or more photofragments, have provided significant insight into the relevant constraints.³⁶ However, systems that show behavior purely consistent with a statistical theory at a global level may, upon more detailed examination at the correlated level, be governed by physical processes that are distinctly

nonrandom.^{16,37} Correlated studies provide highly stringent tests of such proposed dissociation models. In the present work, we have examined the partitioning of the vibrational energy at the correlated level in a room temperature sample. When compared to different statistical predictions, these distributions provide insight into not only the evolution of the parent internal energy but also the physical processes that dictate the final product state distributions.

Of particular interest with respect to NCNO is the validity of SSE theory, originally proposed by Wittig and co-workers, to describe the correlated state distributions.¹⁴ In SSE theory, the vibrational product distribution is assumed to be determined early in the reaction, well before the “loose” outer transition state. The rotational energy is then allowed to couple at longer range, resulting in PST rotational distributions in each vibrational coincident channel. SSE was found to effectively reproduce measured global CN and NO rotational distributions derived from the photodissociation of jet-cooled NCNO at several wavelengths. A later study utilized laser induced fluorescence (LIF) to measure nascent Doppler profiles of CN radicals from NCNO in order to test SSE at a correlated level.⁸ SSE was found to fit the resulting Doppler profiles well for several rotational states at dissociation energies ranging from 411 to 2348 cm^{-1} . However, the linewidth of the probe laser used in these experiments was estimated to be $\sim 0.07 \text{ cm}^{-1}$, and the typical CN linewidth was $\sim 0.1 \text{ cm}^{-1}$, effectively limiting the overall velocity resolution of the LIF experiments. Although the authors used the trough between the F_1 and F_2 spin components to increase their resolution, subtle differences between the shapes of the partial contributions corresponding to the distinct vibrational channels would have been difficult to discern from changes in the correlated vibrational branching ratios. In addition, the lines were measured in the $B-X$ electronic transition, for which no Q -branch is present. This precluded measurement of the $\mathbf{v}-\mathbf{J}$ correlations, which are expected to be large in a jet-cooled sample and would tend to bias the R -branch fits toward apparently larger $v=1$ vibrational branching ratios.³³

The use of a thermal sample provides an additional important test of the treatment of the K -rotor within the SSE model. Optical excitation of a thermal sample prepares molecules with a fixed vibrational energy and a thermal distribution of J and K . If the K -rotor is active in the thermal samples, the NCNO vibrational reservoir is allowed to exchange energy with the K -rotor until the K distribution is uniform. In the case of a prolate symmetric top, this results in a net decrease in the total vibrational energy and thus a lower $v=1$ probability. However, an inactive K -rotor does not couple with the vibrational reservoir, and the vibrational energy remains constant throughout the reaction, irrespective of the initial parent rotational motion. Therefore, the correlated measurements may be able to distinguish between the predictions of a K -conserved and K -scrambled model in a thermal sample. Previous studies which have applied the SSE model to NCNO photodissociation have focused on jet-cooled samples, where the parent rotational energy is small and the difference between the K -conserved and K -scrambled models is minor. We have explicitly incorporated the rotational energy into the phase space calculation of

the basis functions as noted above. Figure 5 shows two SSE curves: one where the *K*-rotor is considered conserved, resulting in no change in the vibrational energy reservoir, and one allowing *K*-scrambling, which results in changes in the vibrational reservoir. The latter model involves a weighted average of the *J*, *K* states, and both models include contributions from the parent vibrational energy, which was weighted using a thermally averaged Beyer–Swinehart algorithm.

The agreement between the measured vibrational branching fractions and the predicted *K*-conserved SSE values is very good but is poor for both the PST and *K*-scrambled SSE predictions. Physically the SSE model describes the exchange of energy between conserved modes within a vibrational reservoir up to the inner transition state. The observation that a *K*-conserved model fits our measurements suggests that *K* is a good quantum number until the conserved modes cease to exchange energy. This suggests that implementation of RRKM theory to calculate dissociation rates at these energies should treat the *K*-rotor as inactive in the reactant. The high resolution of the Doppler spectra and the ability to accurately fit a thermal sample weighted by a simple distribution derived from a Beyer–Swinehart algorithm gives us confidence that SSE theory describes the dynamics at 520 nm well. We have avoided a detailed correlated vibrational analysis on the 532 nm Doppler spectra, since a 532 nm photon is below the threshold for formation of $v=1$ NO from cold parent molecules. Any $v=1$ NO molecules are exclusively derived from only hot bands, and the resulting Doppler lineshapes are therefore exquisitely sensitive to the initial parent distribution of energies.

V. CONCLUSION

The photodissociation of NCNO at 520 and 532 nm has been examined using transient frequency modulation Doppler spectroscopy in order to study vector and scalar correlations in the dissociation. A small correlation between \mathbf{v} and \mathbf{J} was observed corresponding to $\beta_0^0(22)$ bipolar moments ranging from 0.00 ± 0.02 to -0.03 ± 0.02 at 532 nm and 0.00 ± 0.02 to -0.01 ± 0.02 at 520 nm. These were well described by a helicity unrestricted PST formulation at both wavelengths. Restrictions on the total helicity produced significantly more negative $\mathbf{v}-\mathbf{J}$ correlations, providing evidence for approximate *K*-scrambling beyond the outer transition state. The correlated vibrational branching ratios were also measured using PST rotational distributions to generate the correlated basis sets. The measured branching ratios are well described by a *K*-conserved SSE model at 520 nm, implying efficient *K*-mixing between the inner and outer transition states. Future experiments, currently underway, will study these various facets of NCNO photodissociation and will include molecular beam experiments to reduce the blurring arising from the initial parent motion. These experiments will further probe the validity of PST for the correlated rotational distributions and SSE for the correlated vibrational distributions in a low-temperature sample.

ACKNOWLEDGMENTS

The authors would like to thank Dr. H. Reisler and Dr. C. X. W. Qian for information regarding the NCNO synthesis. The authors also acknowledge Dr. G. E. Hall, Dr. S. J. Klippenstein, and Dr. R. R. Lucchese for helpful discussions. This research was supported by a grant from the Robert A. Welch Foundation (Grant No. A-1386).

APPENDIX: ROTATIONAL DEPolarIZATION

The rotational depolarization correction to the center-of-mass (COM) correlations ($\mathbf{u}\cdot\mathbf{J}$) may be estimated by applying the azimuthally averaged addition (AAA) theorem³⁸ to the COM correlation,

$$\langle P_2(\mathbf{v}\cdot\mathbf{J}) \rangle = \langle P_2(\mathbf{u}\cdot\mathbf{v}) \rangle \langle P_2(\mathbf{u}\cdot\mathbf{J}) \rangle,$$

where \mathbf{u} and \mathbf{v} are the relative velocity axes before and after rotation, respectively, \mathbf{J} is the fragment rotational angular momentum vector, and $P_2(x)$ is the second Legendre polynomial. The depolarization factor, $\langle P_2(\mathbf{u}\cdot\mathbf{v}) \rangle$, is calculated semiclassically from the initial relative velocity and the tangential velocity of the center-of-mass of the detected fragment. The tangential velocity is calculated from the total parent rotational quantum number, J_0 , taking into account rotation about the *K*-axis, which is given by the total fragment helicity, Λ . The depolarization factor is calculated for each possible set of parent vibrational and rotational quantum numbers and weighted accordingly using a Boltzmann distribution of rotations and a Boltzmann-weighted vibrational distribution calculated using a Beyer–Swinehart algorithm.

Shown in Fig. 6 are calculated depolarization factors for the dissociation of room-temperature NCNO at 532 nm when probing $N=17$ CN radicals. The rotational temperature used to calculate the Boltzmann distributions was 295 K, and these factors were calculated using the ground vibrational state for the parent molecule. For low coincident NO rota-

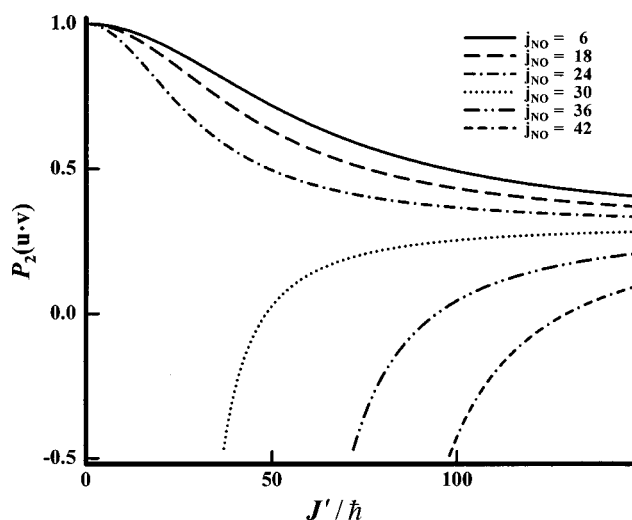


FIG. 6. Rotational depolarization factors as a function of rotational angular momentum about the short symmetry top axis, J' (units of \hbar). These depolarization factors describe the dissociation of NCNO at 532 nm by probing the CN radicals with $N=17$ at 295 K.

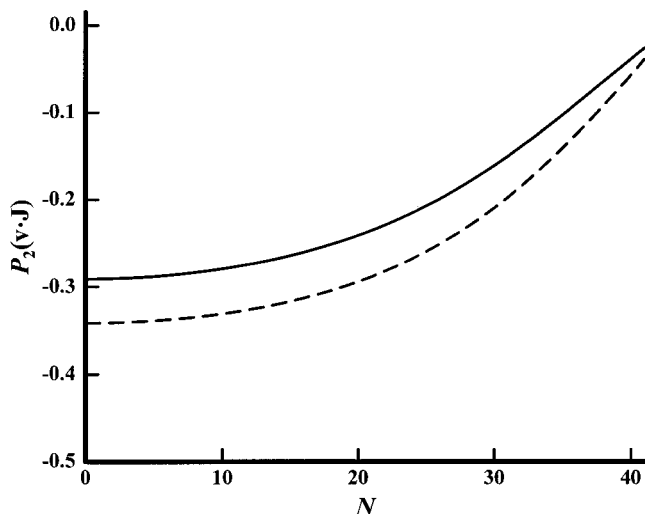


FIG. 7. Calculated values of the translationally and rotationally depolarized v - J correlation for the 355 nm photodissociation of NO_2 at 295 K. The solid line represents the v - J correlations with both the translational and rotational corrections, and the dashed line represents the v - J correlations with only the translational correction.

tional states, the depolarization factors decrease slowly with increasing values of J_0 . However, as the coincident fragments become higher in energy, less translational energy is available, and the rotational depolarization becomes more important. When the coincident rotational quantum number, N_{NO} , exceeds 30, products may only be observed from rotationally excited parent molecules. For these coincident states, the depolarization factor begins at -0.50 at threshold and increases smoothly for each coincident NO state. In practice, this correction is applied to the calculated PST v - J correlations, and the translational depolarization correction is subsequently applied to these values.

As a test of the applicability of this depolarization method, we have calculated rotational depolarization factors for the photodissociation of NO_2 at 355 nm in a room temperature bulb. Since NO_2 is triatomic, a limiting v - J correlation of -0.5 is expected for all J states in the absence of parent translational and rotational motion. This provides an ideal method for directly measuring the depolarization factors. Baker *et al.* have measured v - J correlations for NO_2 photodissociation under these conditions using laser induced fluorescence (LIF) detection of the NO products.³⁹ For $j_{\text{NO}} = 14.5$, the authors measured values for $\beta_0^0(22)$ of -0.31 ± 0.12 and -0.25 ± 0.12 for the F_1 and F_2 spin states, respectively. Shown in Fig. 7 are calculated depolarization factors as a function of the detected NO rotational state. The solid line includes both translational and rotational contributions, while the dashed line shows the effect of the translational depolarization alone. The depolarized value of the v - J correlation at $j_{\text{NO}} = 14.5$ was calculated to be -0.27 , in good agreement with the experimentally measured correlations.

¹J. Pfab, J. Häger, and W. Krieger, *J. Chem. Phys.* **78**, 266 (1983).

²I. Nadler, J. Pfab, G. Radhakrishnan, H. Reisler, and C. Wittig, *J. Chem. Phys.* **79**, 2088 (1983).

³I. Nadler, J. Pfab, H. Reisler, and C. Wittig, *J. Chem. Phys.* **81**, 653 (1984).

⁴I. Nadler, H. Reisler, M. Noble, and C. Wittig, *Chem. Phys. Lett.* **108**, 115 (1984).

⁵I. Nadler, M. Noble, H. Reisler, and C. Wittig, *J. Chem. Phys.* **82**, 2608 (1985).

⁶I. Nadler, H. Reisler, M. Noble, and C. Wittig, *Chem. Phys. Lett.* **84**, 115 (1984).

⁷C. X. W. Qian, M. Noble, I. Nadler, H. Reisler, and C. Wittig, *J. Chem. Phys.* **83**, 5573 (1985).

⁸C. X. W. Qian, A. Ogai, H. Reisler, and C. Wittig, *J. Chem. Phys.* **90**, 209 (1989).

⁹L. R. Khundkar, J. L. Knee, and A. H. Zewail, *J. Chem. Phys.* **87**, 77 (1987).

¹⁰S. J. Klippenstein, L. R. Khundkar, A. H. Zewail, and R. A. Marcus, *J. Chem. Phys.* **89**, 4761 (1988).

¹¹S. J. Klippenstein, *J. Chem. Phys.* **94**, 6469 (1991).

¹²S. J. Klippenstein, *J. Chem. Phys.* **101**, 1996 (1994).

¹³P. Pechukas and J. C. Light, *J. Chem. Phys.* **42**, 3281 (1965); C. E. Klots, *J. Phys. Chem.* **75**, 1526 (1971); J. Troe, *J. Chem. Phys.* **79**, 6017 (1983).

¹⁴C. Wittig, I. Nadler, H. Reisler, M. Noble, J. Catanzarite, and G. Radhakrishnan, *J. Chem. Phys.* **83**, 5581 (1985).

¹⁵W. L. Hase, *Acc. Chem. Res.* **31**, 659 (1998).

¹⁶S. W. North and G. E. Hall, *J. Chem. Phys.* **106**, 60 (1997).

¹⁷S. W. North, A. J. Marr, A. Furlan, and G. E. Hall, *J. Phys. Chem. A* **101**, 9224 (1997).

¹⁸R. Li, A. Derecskei-Kovacs, and S. W. North, *Chem. Phys.* **254**, 309 (2000).

¹⁹R. Li, W. S. McGivern, and S. W. North, *Chem. Phys. Lett.* **334**, 47 (2001).

²⁰E. A. Dorko, P. H. Flynn, U. Grimm, K. Scheller, and G. W. Maeller, *J. Phys. Chem.* **81**, 2088 (1977).

²¹J. R. Morton and H. W. Wilcox, *Inorg. Synth.* **4**, 48 (1953).

²²S. W. North and G. E. Hall, *Annu. Rev. Phys. Chem.* **51**, 243 (2000).

²³R. N. Dixon, *J. Chem. Phys.* **85**, 1866 (1986).

²⁴S. W. North, A. J. Marr, A. Furlan, and G. E. Hall, *J. Phys. Chem. A* **101**, 9224 (1997).

²⁵W. H. Press, S. A. Teukolsky, W. T. Vetterling, and B. P. Flannery, *Numerical Recipes in Fortran*, 2nd ed. (Cambridge University Press, New York, 1992).

²⁶C. Taatjes, J. Cline, and S. Leone, *J. Chem. Phys.* **93**, 6554 (1990).

²⁷C. G. Morgan, M. Drabbels, and A. M. Wodtke, *J. Chem. Phys.* **104**, 7460 (1996).

²⁸Since the v - J correlations in the present paper were found to be small, we have tested this procedure on previously obtained data from NCCN (Ref. 16), which is characterized by significantly higher values of $\beta_0^0(22)$. Despite the significant differences between the Q - and R -branches for NCCN at early times, the late time data show very good overlap, and we are confident this procedure is a valid means for ensuring the correct widths from scan to scan.

²⁹T. Baer and W. L. Hase, *Unimolecular Reaction Dynamics* (Oxford, New York, 1996).

³⁰As suggested in Ref. 29, the value of the C_6 term was determined from the bond energy and the equilibrium bond distance. The value of C_6 used in the present work is $6.37 \times 10^6 \text{ cm}^{-1} \text{ \AA}^6$.

³¹P. Pechukas and J. C. Light, *J. Chem. Phys.* **42**, 3281 (1965).

³²D. Cerny, R. Bacis, G. Guelachvili, and F. Roux, *J. Mol. Spectrosc.* **73**, 154 (1978).

³³S. W. North and G. E. Hall, *J. Chem. Phys.* **104**, 1864 (1996).

³⁴S. W. North and G. E. Hall, *Ber. Bunsenges. Phys. Chem.* **101**, 459 (1997).

³⁵NCNO is nonlinear in the ground state with rotational constants $A = 2.71 \text{ cm}^{-1}$, $B = 0.180 \text{ cm}^{-1}$, and $C = 0.168 \text{ cm}^{-1}$; R. Dickinson, G. W. Kirby, J. G. Sweeny, and J. K. Tyler, *J. Chem. Soc. Faraday Trans. 2* **74**, 1393 (1978).

³⁶W. H. Green, Jr., C. B. Moore, and W. F. Polik, *Annu. Rev. Phys. Chem.* **43**, 591 (1992).

³⁷M. L. Costen, H. Katayanagi, and G. E. Hall, *J. Phys. Chem. A* **104**, 10247 (2000).

³⁸J. D. Barnwell, J. G. Loesser, and D. R. Herschbach, *J. Phys. Chem.* **87**, 2781 (1983).

³⁹R. P. Baker, M. L. Costen, G. Hancock, G. A. D. Ritchie, and D. Summerfield, *Phys. Chem. Chem. Phys.* **2**, 661 (2000).